STRUCTURAL BIOLOGY
ISSN 2059-7983

Nogo Receptor crystal structures with a native disulfide pattern suggest a novel mode of self-interaction

Matti F. Pronker,‡ Roderick P. Tas,§ Hedwich C. Vlieg and Bert J. C. Janssen*

Crystal and Structural Chemistry, Bijvoet Center for Biomolecular Research, Department of Chemistry, Faculty of Science, Utrecht University, Padualaan 8, 3584 CH Utrecht, The Netherlands. *Correspondence e-mail: b.j.c.janssen@uu.nl

Received 23 July 2017
Accepted 25 September 2017

Edited by Z. S. Derewenda, University of Virginia, USA

‡ Current address: Division of Neurobiology, MRC Laboratory of Molecular Biology, University of Cambridge, Francis Crick Avenue, Cambridge CB2 0HQ, England.
§ Current address: Cell Biology, Department of Biology, Faculty of Science, Utrecht University, Padualaan 8, 3584 CH Utrecht, The Netherlands.

Keywords: neuronal plasticity; myelin-associated inhibitors; X-ray crystallography; small-angle X-ray scattering; analytical ultracentrifugation; Nogo Receptor.

PDB references: NgRa-1, 5o0k; NgRa-2, 5o0l; NgRa-3, 5o0m; NgRa-4, 5o0n; NgRa-5, 5o0o; NgRb-1, 5o0p; NgRb-2, 5o0q; NgRb-3, 5o0r

Supporting information: this article has supporting information at journals.iucr.org/d

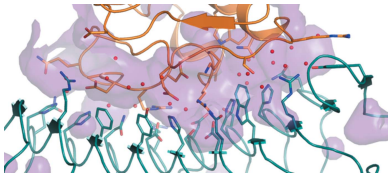

© 2017 International Union of Crystallography

The Nogo Receptor (NgR) is a glycophosphatidylinositol-anchored cell-surface protein and is a receptor for three myelin-associated inhibitors of regeneration: myelin-associated glycoprotein, Nogo66 and oligodendrocyte myelin glycoprotein. In combination with different co-receptors, NgR mediates signalling that reduces neuronal plasticity. The available structures of the NgR ligand-binding leucine-rich repeat (LRR) domain have an artificial disulfide pattern owing to truncated C-terminal construct boundaries. NgR has previously been shown to self-associate *via* its LRR domain, but the structural basis of this interaction remains elusive. Here, crystal structures of the NgR LRR with a longer C-terminal segment and a native disulfide pattern are presented. An additional C-terminal loop proximal to the C-terminal LRR cap is stabilized by two newly formed disulfide bonds, but is otherwise mostly unstructured in the absence of any stabilizing interactions. NgR crystallized in six unique crystal forms, three of which share a crystal-packing interface. NgR crystal-packing interfaces from all eight unique crystal forms are compared in order to explore how NgR could self-interact on the neuronal plasma membrane.

1. Introduction

The Nogo Receptor (NgR) is a neuronal cell surface-expressed glycophosphatidylinositol (GPI)-anchored protein receptor for ligands that negatively regulate plasticity in the central nervous system (CNS) (Mironova & Giger, 2013; Baldwin & Giger, 2015; McGee & Strittmatter, 2003; Akbik *et al.*, 2012). Knockout of NgR results in prolonged periods of ocular dominance plasticity (McGee *et al.*, 2005; Stephany *et al.*, 2016) and anatomical plasticity at dendritic spines and synapses (Lee *et al.*, 2008; Raiker *et al.*, 2010; Akbik *et al.*, 2013). NgR is part of receptor complexes that mediate signalling by three myelin-associated inhibitors (MAIs) that inhibit neurite sprouting and outgrowth, and collapse axonal growth cones upon injury in the CNS (Mironova & Giger, 2013; Baldwin & Giger, 2015; McGee & Strittmatter, 2003; Akbik *et al.*, 2012). The three structurally unrelated MAIs myelin-associated glycoprotein (MAG), Nogo66 and oligodendrocyte myelin glycoprotein (OMgp) all bind and signal through NgR to inhibit neurite outgrowth and collapse axonal growth cones (Fournier *et al.*, 2001; Liu *et al.*, 2002; Wang, Koprivica *et al.*, 2002). These three MAIs bind to the N-terminal leucine-rich repeat (LRR) domain of NgR (Wang, Koprivica *et al.*, 2002; Liu *et al.*, 2002; Fournier *et al.*, 2002; Barton *et al.*, 2003; Venkatesh *et al.*, 2005; Laurén *et al.*, 2007; Robak *et al.*, 2009). C-terminal to the NgR LRR domain is a heavily glycosylated stalk that contains a disulfide-linked loop (Wen *et al.*, 2005) followed by a GPI-anchoring sequence that

is replaced by a GPI anchor in mature NgR. The stalk of NgR is required but not sufficient for signal transduction, and replacing the GPI anchor with a transmembrane helix results in reduced sensitivity of neurons to MAI ligands (Fournier *et al.*, 2002).

Since NgR is GPI-anchored and lacks an intracellular domain for signal transduction into the neuron, it forms signalling complexes together with four different transmembrane co-receptors: the neurotrophin receptor p75 (Wong *et al.*, 2002; Wang, Kim *et al.*, 2002), its homologue TROY, LRR and immunoglobulin-like domain-containing NgR-interacting protein 1 (LINGO-1; Mi *et al.*, 2004), and its homologue amphoterin-induced gene and open reading frame 3 (AMIGO3). NgR forms complexes with either p75 or TROY and either LINGO-1 or AMIGO3 to mediate MAI signalling.

Structures have been solved of the LRR domain of NgR (Barton *et al.*, 2003; He *et al.*, 2003) as well as its paralogue NgR2 (Semavina *et al.*, 2011). However, the currently available NgR structures were obtained from truncated constructs [residues 26–310 for Protein Data Bank (PDB) entry 1ozn and 27–311 (He *et al.*, 2003) for PDB entry 1p8t (Barton *et al.*, 2003)] that result in an artificial disulfide pattern in the C-terminal LRR capping region (Wen *et al.*, 2005). In these structures, a disulfide bond is observed between cysteines Cys266 and Cys309 (Barton *et al.*, 2003; He *et al.*, 2003), whereas in full-length NgR Cys266 forms a disulfide with Cys335 and Cys309 with Cys336 (mouse NgR numbering; see Fig. 1) as determined by NgR digestion and subsequent mass spectrometry of the peptides (Wen *et al.*, 2005). This generates an extra disulfide-enclosed segment between Cys309 and Cys335 (residues 310–334; hereafter referred to as the C-terminal segment). The structure of this native disulfide-linked C-terminal segment is unknown. The cysteines Cys335 and Cys336 that are responsible for this arrangement are conserved in NgR orthologues (Fig. 1, bottom panel) but are not conserved in the NgR paralogues NgR2 and NgR3. Deletion of this loop (residues 314–335) has been reported to selectively increase the binding of Nogo66 and OMgp, but not of MAG, to NgR (Robak *et al.*, 2009). A chimeric protein consisting of the LRR of NgR, in which this loop is replaced with a 13-amino-acid nonloop sequence from the stalk of NgR2, binds more strongly to all three MAIs than either NgR or NgR2 (Robak *et al.*, 2009). The C-terminal segment is expected to be on the convex side of the LRR next to the C-terminal LRR cap (Wen *et al.*, 2005). However, mutagenesis studies, as well as evolutionary conservation, suggest that it is the concave rather than the convex side of the NgR LRR that is involved in binding all three MAIs as well as LINGO-1 (Laurén *et al.*, 2007; He *et al.*, 2003). Thus, it remains unclear how the disulfide pattern of the C-terminal LRR capping domain and the extra C-terminal loop influence the binding of MAI ligands.

Three different NgR truncation constructs, corresponding to the artificially short LRR (residues 27–310), the LRR including the C-terminal segment (residues 27–344) and a construct including most of the glycosylated stalk (residues 27–431) have been compared in cell-binding experiments to determine the region necessary for p75 and TROY binding. For both p75 and TROY, binding was observed with just the short LRR of NgR, but the affinity was increased by including the C-terminal segment and further enhanced for the nearly full extracellular construct (Shao *et al.*, 2005). Other studies found that the short LRR does not support p75 binding, whereas the full extracellular segment of NgR does (Wang, Kim *et al.*, 2002; He *et al.*, 2003). These results confirm earlier studies showing that the membrane-attached NgR LRR without the stalk is not sufficient for Nogo66-induced signalling (Fournier *et al.*, 2002). Taken together, these data indicate that the artificially short NgR LRR domain supports the binding of the three MAI ligands (Wang, Koprivica *et al.*, 2002; Liu *et al.*, 2002; Fournier *et al.*, 2002; Barton *et al.*, 2003; Venkatesh *et al.*, 2005; Laurén *et al.*, 2007; Robak *et al.*, 2009), but that the C-terminal loop and the glycosylated stalk are required for efficient co-receptor binding and signal transduction.

NgR has been shown to self-interact *via* its LRR domain (Fournier *et al.*, 2002; Saha *et al.*, 2011; Barton *et al.*, 2003) at the plasma membrane (Fournier *et al.*, 2002; Barton *et al.*, 2003). These assemblies have previously been suggested to represent an inactive signalling state as they can form in the absence of MAI ligands (Barton *et al.*, 2003). However, the structural basis of this interaction remains elusive, as the available NgR structures do not have any crystal-packing interfaces in common (Barton *et al.*, 2003; He *et al.*, 2003; Weinreb *et al.*, 2010).

Although a structural model has been proposed for the 310–334 segment and its manner of interaction with the rest of NgR (Wen *et al.*, 2005), this model is not supported by any experimental data. Also, it is not clear how the NgR LRR self-associates (Fournier *et al.*, 2002; Saha *et al.*, 2011; Barton *et al.*, 2003). Here, we describe six independent crystal structures of NgR with native disulfide bonds, show that the C-terminal segment forms a flexible loop in the absence of any stabilizing ligands and propose a novel mode of NgR self-interaction.

2. Methods

2.1. Generation of constructs and mutagenesis

Mouse NgR constructs were generated by polymerase chain reaction (PCR) with the cDNA (IMAGE clone 6397765) as a template and primers to start at UniProt residue 26 (after the signal peptide) and end at residue 337 (NgRa) or 348 (NgRb). Mutants were made by a two-step PCR using elongated overlapping primers. All constructs were subcloned using BamHI/NotI sites in pUPE107.03 (cystatin secretion signal peptide, C-terminal His_6 tag; U-Protein Express).

2.2. Large-scale expression and purification

Constructs were transiently expressed in *N*-acetylglucosaminyltransferase I-deficient ($GnTI^-$) Epstein–Barr virus nuclear antigen I (EBNA1)-expressing HEK293 cells in suspension (U-Protein Express). DNA titration by dilution with non-expressing PCR4 DNA was used to boost expression

levels, similar to a previously described approach (Halff *et al.*, 2014). DNA was diluted 25× for NgRa, 100× for NgRb, 5× for NgRb D111R or 5× for NgRb R300E. The medium was harvested 6 d after transfection and the cells were spun down

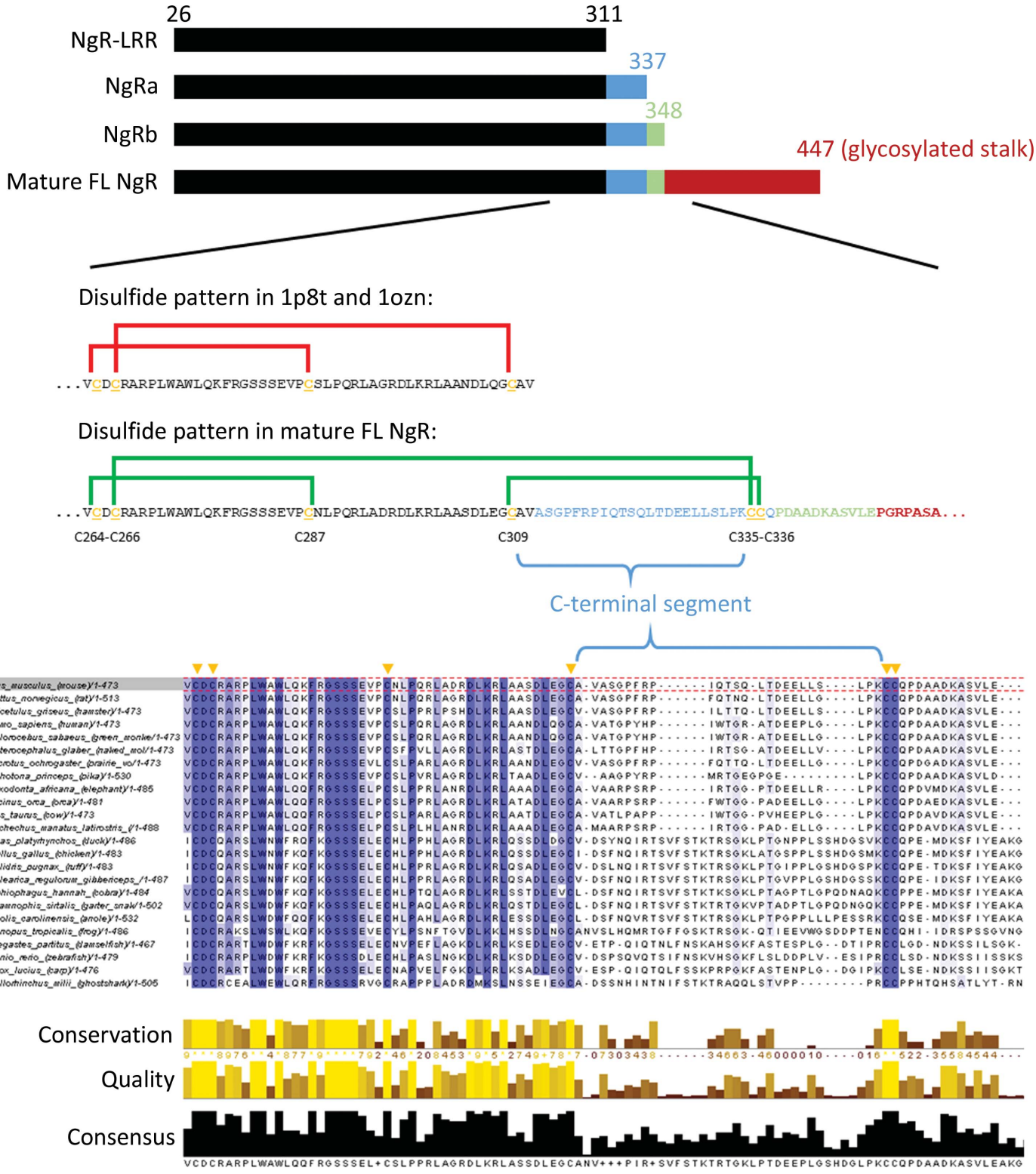

Figure 1
Rationale for construct design. The C-terminal cap of the LRR of NgR in the available structures (Barton *et al.*, 2003; He *et al.*, 2003) has an artificial disulfide pattern owing to construct boundaries (Wen *et al.*, 2005). Therefore, longer constructs of the NgR LRR including Cys335 and Cys336 were generated (NgRa and NgRb) that include an extra C-terminal segment (blue) that is enclosed by the Cys266–Cys335 and Cys309–Cys336 disulfides. NgRb also includes a relatively conserved and hydrophobic sequence C-terminal to these cysteines (green); the bottom panel shows a sequence alignment of this region in NgR orthologues. Amino acids are coloured by percentage identity (blue is more conserved).

by 10 min of centrifugation at 1000*g*. The supernatant was concentrated fivefold and diafiltered against 500 m*M* NaCl, 25 m*M* 4-(2-hydroxyethyl)-1-piperazineethanesulfonic acid (HEPES) pH 7.5 using a QuixStand benchtop system (GE Healthcare) with a 10 kDa molecular-weight cutoff (MWCO) membrane. Cellular debris was spun down for 10 min at 9500*g* and the supernatant was filtered with a glass-fibre prefilter (Minisart, Sartorius). The protein was purified by nickel–nitrilotriacetic acid (Ni–NTA) affinity chromatography followed by size-exclusion chromatography (SEC) on a Superdex 75 HiLoad 16/60 column (GE Healthcare) equilibrated with SEC buffer (150 m*M* NaCl, 20 m*M* HEPES pH 7.5). The protein was concentrated to 10–15 mg ml^{-1} using a 10 kDa MWCO concentrator prior to plunge-freezing in liquid nitrogen and storage at 193 K.

2.3. Crystallization and data collection

Glycosylated as well as enzymatically deglycosylated protein was used for crystallization. Deglycosylation was performed by overnight treatment with Endo H$_f$ [1.0 × 10^6 U ml^{-1}, New England Biolabs; added to 1:100(*v*:*v*)] at 298 K (NgRa) or 310 K (NgRb). The completeness of deglycosylation was analyzed by SDS–PAGE. Sitting-drop vapour diffusion at 277 or 291 K was used for all crystallization trials by mixing 150 nl protein solution with 150 nl reservoir solution. Crystallization was typically performed at concentrations of 10–13 mg ml^{-1}.

NgRa-1 was the result of a co-crystallization trial with Endo H$_f$-deglycosylated mouse TROY cysteine-rich domains 1–3 (UniProt Q9JLL3, residues 30–152), mixed at equimolar stoichiometry in SEC buffer. NgRa was also Endo H$_f$-deglycosylated. Crystals were grown at 291 K in a condition consisting of 0.05 *M* citric acid pH 5.0, 15%(*w*/*v*) polyethylene glycol (PEG) 6000.

NgRa-2 was the result of a co-crystallization trial with the Endo H$_f$-deglycosylated extracellular domain of mouse MAG (UniProt P20917, residues 20–508), mixed at equimolar stoichiometry in SEC buffer. NgRa was also Endo H$_f$-deglycosylated. Crystals were grown at 277 K in a condition consisting of 0.5 *M* LiCl, 0.05 *M* citric acid pH 4.0, 15%(*w*/*v*) PEG 6000.

NgRa-3 crystals were grown at 291 K in a condition consisting of 0.05 *M* sodium malonate:imidazole:boric acid (MIB) buffer (2:3:3 molar ratio of sodium malonate:imidazole:boric acid) pH 5.0, 12.5%(*w*/*v*) PEG 1500. NgRa was Endo H$_f$-deglycosylated for NgRa-3. The NgRa-3 crystal was soaked with 10 m*M* *N*-acetylneuraminic acid prior to cryoprotection and cooling.

NgRa-4 was the result of a co-crystallization trial with mouse Nogo54, an extracellular construct derived from the NgR ligand Nogo-A (UniProt Q99P72, residues 1025–1078). Nogo54 was purified in 150 m*M* NaCl, 20 m*M* HEPES pH 7.0 at a concentration of 3.3 mg ml^{-1} and was mixed in a 1:1 molar ratio with Endo H$_f$-deglycosylated NgRa at a concentration of 10 mg ml^{-1}. Crystals were grown at 291 K in a condition consisting of 0.2 *M* ammonium sulfate, 0.1 *M* bis-tris pH 6.5, 25%(*w*/*v*) PEG 3350.

Table 1
SAXS parameters of NgR constructs at different concentrations.

Glyc., glycosylated; deglyc., deglycosylated using Endo H$_f$.

	M_m (kDa)	Concentration (μ*M*)	R_g (nm)	M_m based on I_0 (kDa)	D_{max} (nm)	Porod volume (nm^3)
NgRb wt glyc.	40.6	130	3.28	44.4	15.2	75.0
NgRb wt glyc.	40.6	57	2.90	37.1	11.6	67.3
NgRb wt glyc. SEC	40.6	NA	2.84	NA	8.7	64.2
NgRb D111E glyc.	40.6	123	3.42	43.6	16.0	73.3
NgRb D111E glyc.	40.6	57	2.97	40.6	12.9	67.3
NgRb R300E glyc.	40.6	126	3.26	42.5	14.6	70.4
NgRb R300E glyc.	40.6	58	2.90	37.1	11.5	65.5
NgRb wt deglyc.	37.6	136	3.61	48.1	16.3	72.4
NgRb wt deglyc.	37.6	63	3.11	36.4	11.6	57.6
NgRb R300E deglyc.	37.6	143	3.02	49.0	12.0	71.3
NgRb R300E deglyc.	37.6	59	2.80	41.2	10.9	65.2
NgRa wt deglyc.	36.5	151	3.62	52.9	13.8	81.4
NgRa wt deglyc.	36.5	57	2.94	37.1	12.1	55.8

NgRa-5 crystals were grown at 277 K in a condition consisting of 2.5 *M* NaCl, 100 m*M* sodium acetate/acetic acid pH 4.5, 200 m*M* Li_2SO_4. NgRa was Endo H$_f$-deglycosylated for NgRa-5.

NgRb-1 crystals were grown at 277 K in a condition consisting of 0.05 *M* citric acid, 0.05 *M* bis-tris propane pH 5.0, 16%(*w*/*v*) PEG 3350. NgRb was Endo H$_f$-deglycosylated for NgRb-1.

NgRb-2 crystals were grown at 291 K in a condition consisting of 0.2 *M* NaH_2PO_4 pH 5, 20%(*w*/*v*) PEG 3350. NgRb was Endo H$_f$-deglycosylated for NgRb-2.

NgRb-3 crystals were grown at 291 K in a condition consisting of 1.8 *M* NaH_2PO_4/K_2HPO_4 pH 5.0. NgRb was Endo H$_f$-deglycosylated for NgRb-2.

Crystals were cryoprotected with reservoir solution supplemented with 25% glycerol before plunge-cooling them in liquid nitrogen. All data were collected at 100 K on the following beamlines: European Synchrotron Radiation Facility (ESRF) ID23-1 (NgRa-1, NgRa-4, NgRb-1 and NgRb-3), ID23-2 (NgRb-2) and ID29 (NgRa-2), and Swiss Light Source (SLS) X06SA (NgRa-3 and NgRa-5). Data were integrated with *iMosflm* (Battye *et al.*, 2011; NgRa-2, NgRa-4 and NgRa-5) or *XDS* (Kabsch, 2010; NgRa-1, NgRa-3, NgRb1, NgRb2 and NgRb3), and were scaled and merged using the *AIMLESS* pipeline (Evans & Murshudov, 2013; Evans, 2011).

2.4. Structure solution and refinement

All structures were solved by molecular replacement with *Phaser* (McCoy *et al.*, 2007) using PDB entry 1ozn as a search model (He *et al.*, 2003). The structures were modelled by cycles of model building in *Coot* (Emsley & Cowtan, 2004) and refinement using *REFMAC* (Murshudov *et al.*, 2011) and *phenix.refine* (Afonine *et al.*, 2012). Eightfold noncrystallographic symmetry map averaging was used in *Coot* (Emsley & Cowtan, 2004) to obtain better electron-density maps for the C-terminal loop of the NgRa-5 crystal form. Ramachandran statistics were (Ramachandran favoured/allowed/outliers as percentages) 95/5/0 for NgRa-1, 93.5/6.3/0.2 for NgRa-2, 95.7/4.3/0 for NgRa-3, 92.8/6.2/0 for NgRa-4, 95.4/4.6/0 for

NgRa-5, 95.5/4.3/0.2 for NgRb-1, 93.8/6.2/0 for NgRb-2 and 93.3/6.7/0 for NgRb-3.

2.5. Structure analysis

Surface areas were calculated by the *PISA* server (Krissinel & Henrick, 2007). Evolutionary conservation of surface residues was assessed using the *ConSurf* server (Glaser *et al.*, 2003). Binding affinities were predicted by the *PRODIGY* server (Vangone & Bonvin, 2015). All protein structures were visualized using *PyMOL* (Schrödinger).

2.6. Small-angle X-ray scattering

Small-angle X-ray scattering (SAXS) was performed on the ESRF BM29 BioSAXS beamline equipped with a two-dimensional PILATUS 1M detector (DECTRIS, Switzerland), operated at an energy of 12.5 keV. Wild-type NgRb (NgRb wt) and mutants were dialyzed against SEC buffer using a 10 kDa MWCO membrane. Sample concentrations were determined by UV–Vis spectroscopy on a NanoDrop ND-1000 spectrophotometer (see Table 1). SAXS data were collected at 293 K. Ten successive frames of 1 s exposure were collected for each

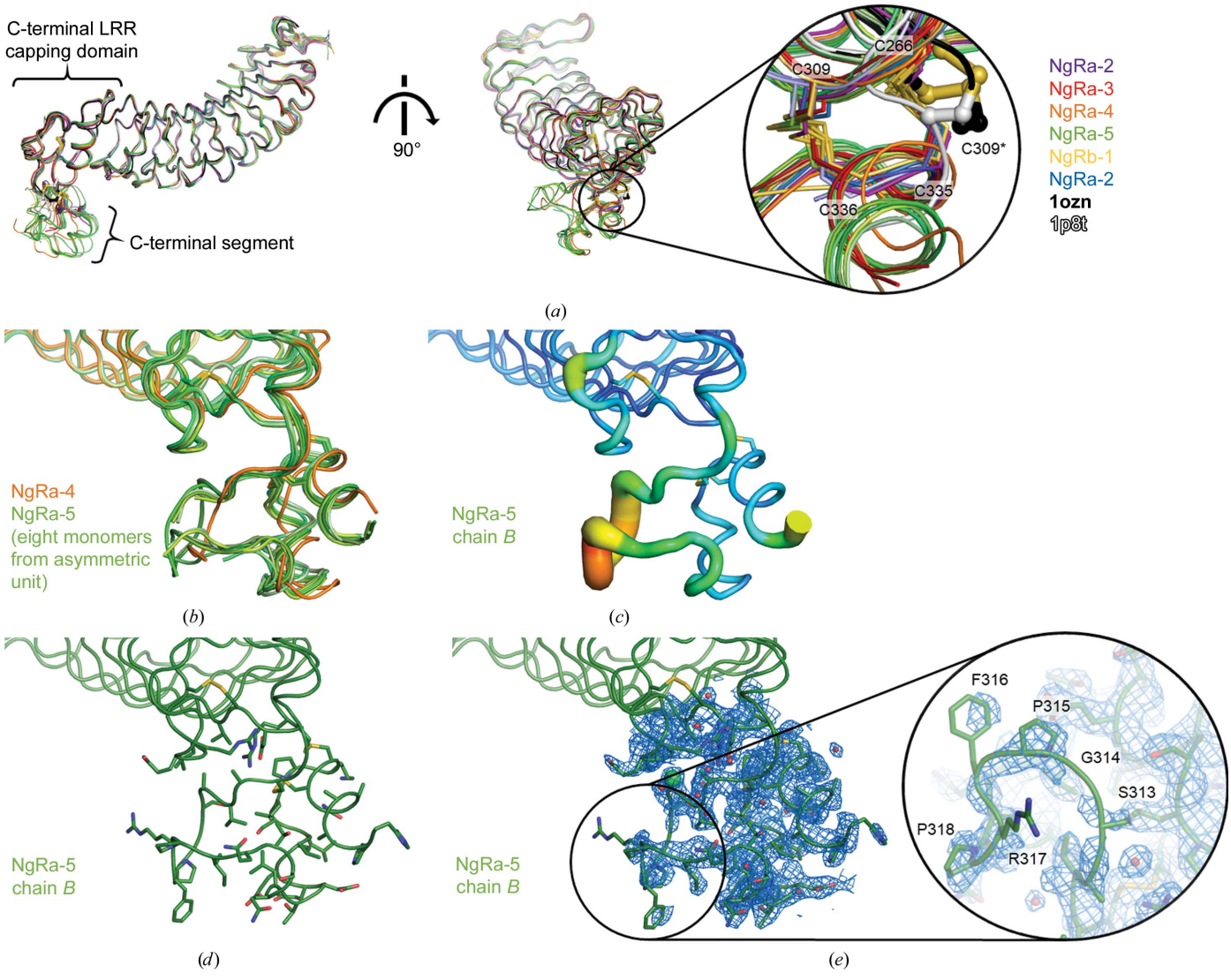

Figure 2
Crystal structures of NgRa and NgRb reveal that the C-terminal loop is mostly flexible. (*a*) The six different independent crystal forms of NgR with the correct disulfide structure are compared with the currently published structures with PDB entries 1p8t (Barton *et al.*, 2003) and 1ozn (He *et al.*, 2003). The structure of the LRR domain is not altered and confirms the alternative disulfide pattern reported previously (Wen *et al.*, 2005). The right panel shows a close-up view of the disulfides as in the previously published structures (thick ball-and-stick representation) and in the structures of the longer NgRa and NgRb constructs (thin sticks). The asterisk indicates the location of Cys309 in PDB entries 1p8t and 1ozn. (*b*) Comparison of the resolved parts of the C-terminal loop in the NgRa-4 and NgRa-5 crystal forms reveals a similar structure which appears to be flexible. In other crystal forms this loop could not be resolved. (*c*) Analysis of the IDPs of the C^{α} atoms in the C-terminal loop for the best-resolved structure of the loop (chain *B* from NgRa-5) confirms that this loop is flexible. A thick tube and red colours represent high *B* factors and a thin tube and blue colours represent low IDPs, using a rainbow gradient. (*d*) The same representation as in (*c*), now showing the side chains as sticks. Most hydrophobic side chains appear to pack together in the C-terminal loop. (*e*) The same representation as in (*d*) but with the $2F_o - F_c$ electron density contoured at 1.0σ. Ordered solvent molecules are shown as red spheres and a chloride ion is shown as a green sphere. A close-up view of residues 313–318 shows that this part of the loop in particular is flexible and poorly resolved.

Table 2
Data-collection and refinement statistics.

Values in parentheses are for the outer shell.

	NgRa-1	NgRa-2	NgRa-3	NgRa-4	NgRa-5	NgRb-1	NgRb-2	NgRb-3
Data collection								
Space group	*C*2	$P2_1$	$P2_12_12_1$	$P4_1$	$P4_12_12$	*C*2	$P2_1$	$P2_12_12_1$
Unit-cell parameters								
a (Å)	151.6	72.91	46.6	90.6	168.5	153.2	132.1	46.7
b (Å)	46.6	38.6	112.1	90.6	168.5	46.9	46.3	111.6
c (Å)	120.7	119.6	115.1	45.6	256.2	121.8	132.2	114.8
$\alpha = \gamma$ (°)	90.0	90.0	90.0	90.0	90.0	90.0	90.0	90.0
β (°)	123.5	106.20	90.0	90.0	90.0	123.6	91.9	90.0
Resolution (Å)	43.78–2.30 (2.39–2.30)	38.60–2.51 (2.62–2.51)	56.03–1.90 (1.94–1.90)	90.63–2.50 (2.61–2.50)	70.39–2.20 (2.24–2.20)	44.01–2.00 (2.05–2.00)	45.94–2.50 (2.58–2.50)	46.73–2.50 (2.64–2.50)
No. of reflections	31309	20826	48250	13084	185934	48789	53288	21264
R_{meas}	0.169 (0.933)	0.137 (0.769)	0.160 (1.306)	0.077 (1.056)	0.148 (1.087)	0.109 (1.329)	0.181 (1.091)	0.252 (0.946)
Mean $I/\sigma(I)$	5.9 (1.5)	12.2 (3.3)	6.0 (1.5)	13.2 (2.4)	11.4 (2.2)	8.5 (1.0)	5.8 (1.0)	3.8 (1.4)
$CC_{1/2}$	0.936 (0.546)	0.992 (0.564)	0.994 (0.503)	0.998 (0.704)	0.998 (0.667)	0.998 (0.593)	0.992 (0.472)	0.981 (0.663)
Completeness (%)	98.7 (98.6)	94.6 (89.6)	99.7 (99.8)	100.0 (100.0)	100.0 (100.0)	99.4 (99.6)	94.8 (96.8)	98.8 (99.8)
Multiplicity	3.7 (3.6)	2.8 (2.6)	4.6 (4.7)	7.4 (7.6)	8.5 (8.7)	3.5 (3.5)	2.6 (2.4)	3.4 (3.7)
Average mosaicity (°)	0.82	0.17	0.31	0.28	0.30	0.15	0.35	0.23
Refinement								
Maximum resolution (Å)	2.3	2.5	1.9	2.5	2.2	2.0	2.5	2.5
R_{work}/R_{free}	0.179/0.234	0.197/0.256	0.179/0.222	0.219/0.248	0.167/0.207	0.183/0.210	0.211/0.261	0.256/0.302
No. of atoms	4942	4751	5397	2572	21913	4959	9660	4597
Average IDPs (Å^2)								
Protein	36.9	52.8	32.6	100.3	39.7	44.1	48.0	50.0
Ligand/ion	64.2/93.1	NA/80.4	NA	NA/131.0	73.8/53.6	77.0/NA	81.2/104.9	57.5/41.0
Water	38.4	36.4	38.5	77.9	41.0	46.9	42.5	41.0
R.m.s. deviations								
Bond lengths (Å)	0.002	0.002	0.003	0.003	0.004	0.006	0.003	0.002
Bond angles (°)	0.650	0.650	0.869	0.658	0.850	1.208	0.569	0.657
MolProbity score	1.35	1.64	0.84	1.64	1.76	1.20	1.74	1.90

sample. The data were radially averaged, normalized to the intensity of the transmitted beam, exposure time and sample concentration, and the scattering of the solvent blank (SEC buffer) was subtracted. The curve was scaled using a BSA reference so that the I_0 represents the molecular mass of NgR. Radiation damage was monitored by comparing curves collected from the same sample; curves that showed signs of radiation damage were discarded. Data were analyzed with *PRIMUS* (Konarev *et al.*, 2003) and *GNOM* (Svergun, 1992) from the *ATSAS* suite (Franke *et al.*, 2017).

2.7. Sedimentation-velocity analytical ultracentrifugation (AUC)

NgRb wt, D111R and R300E were dialyzed against SEC buffer using a 10 kDa MWCO membrane. The protein was diluted with SEC buffer to a concentration of 95 µ*M*. AUC sedimentation-velocity experiments were performed in a Beckman Coulter ProteomeLab XL-A analytical ultracentrifuge using a 3 mm centrepiece, quartz windows and an An-60 Ti rotor (Beckman). Absorption measurements were made at 42 000 rev min^{-1} and 293 K every minute at 280 nm wavelength and with SEC buffer as a reference. $\overline{V}$, buffer density and viscosity were determined by *SEDNTERP* as 0.715 ml g^{-1}, 0.99823 g ml^{-1} and 0.001002 Pa s, respectively. Measurements were analyzed by *SEDFIT* using continuous *c*(*s*) mode (Schuck, 2000; Brown & Schuck, 2006).

3. Results

3.1. Structures of NgR with a native disulfide pattern reveal that the C-terminal segment forms a loop that is flexible in the absence of stabilizing ligands

To study NgR with its native disulfide structure, two constructs were generated that include the extra cysteines that are necessary for correct disulfide formation. Constructs of the NgR LRR truncated after (*Mus musculus*) residues 337 and 348 are hereafter referred to as NgRa and NgRb, respectively. The latter includes an extra 11-amino-acid sequence (PDA-ADKASVLE) that is relatively hydrophobic and conserved among orthologues compared with the rest of the glycosylated stalk (Fig. 1). This NgRb construct is very similar (truncated at residue 348 instead of 344) to the construct that previously showed enhanced binding to p75 and TROY compared with the short LRR, truncated at residue 311, with the artificial disulfide structure (Shao *et al.*, 2005).

Five crystal forms were obtained for NgRa and three for NgRb as glycosylated or Endo H_f-treated versions (Fig. 2). These crystal forms will hereafter be referred to as NgRa-1 to NgRa-5 and NgRb-1 to NgRb-3 (see Tables 2 and 3). A total of 23 new NgR structures were solved considering all NgR molecules in the asymmetric units of all of the crystal forms (Table 3). *C*2 and $P2_12_12_1$ crystal forms were observed for both NgRa (NgRa-1 and NgRa-3, respectively) and NgRb (NgRb-1 and NgRb-3, respectively). NgRa-3 and NgRb-1 diffracted to the highest resolution (1.9 and 2.0 Å, respectively), whereas the lowest maximum resolution of 2.5 Å was obtained for

Table 3
Comparison of crystallization conditions.

	Crystal form equivalent to	Interface 1	Crystallization temperature (K)	Deglycosylated?	Monomers in asymmetric unit	pH
NgRa-1	NgRb-1	Yes	291	Yes	2	5
NgRa-2			277	Yes	2	4
NgRa-3	NgRb-3	Yes	291	Yes	2	5
NgRa-4			291	Glycosylated	1	6.5
NgRa-5			277	Yes	8	4.5
NgRb-1	NgRa-1	Yes	277	Yes	2	5
NgRb-2		Yes	291	Yes	4	5
NgRb-3	NgRa-3	Yes	291	Yes	2	5

NgRa-2, NgRa-4 and NgRb-3. Most often, NgR crystallized as needles in low-pH conditions (pH 4–5), but other morphologies and higher pH values (up to pH 6.5) also occurred (see Table 3). Three crystallization conditions contained NgR ligands or co-receptors in attempts to obtain crystals of complexes, but electron density for these additional molecules was not observed in any of the data sets (see §2 for details).

All structures were solved by molecular replacement using a previously solved structure of the human NgR LRR (He *et al.*, 2003) as a search model. Both previously confirmed N-linked glycans at Asn82 and Asn179 (He *et al.*, 2003) were confirmed in all of our structures, as well as an N-linked glycan at Asn237, which is part of a canonical N*x*S motif for N-linked glycosylation (Fig. 3). Despite the presence of this motif, this N-linked glycan was not observed in the three previously published structures (Barton *et al.*, 2003; He *et al.*, 2003; Weinreb *et al.*, 2010). The native disulfide pattern that was shown by mass spectrometry (Wen *et al.*, 2005), with Cys266–Cys335 and Cys309–Cys336 disulfides instead of the artificial Cys266–Cys309, was confirmed in all our structures. Two cysteines in the glycosylated stalk (Cys419 and Cys429) that are absent in our constructs were shown in

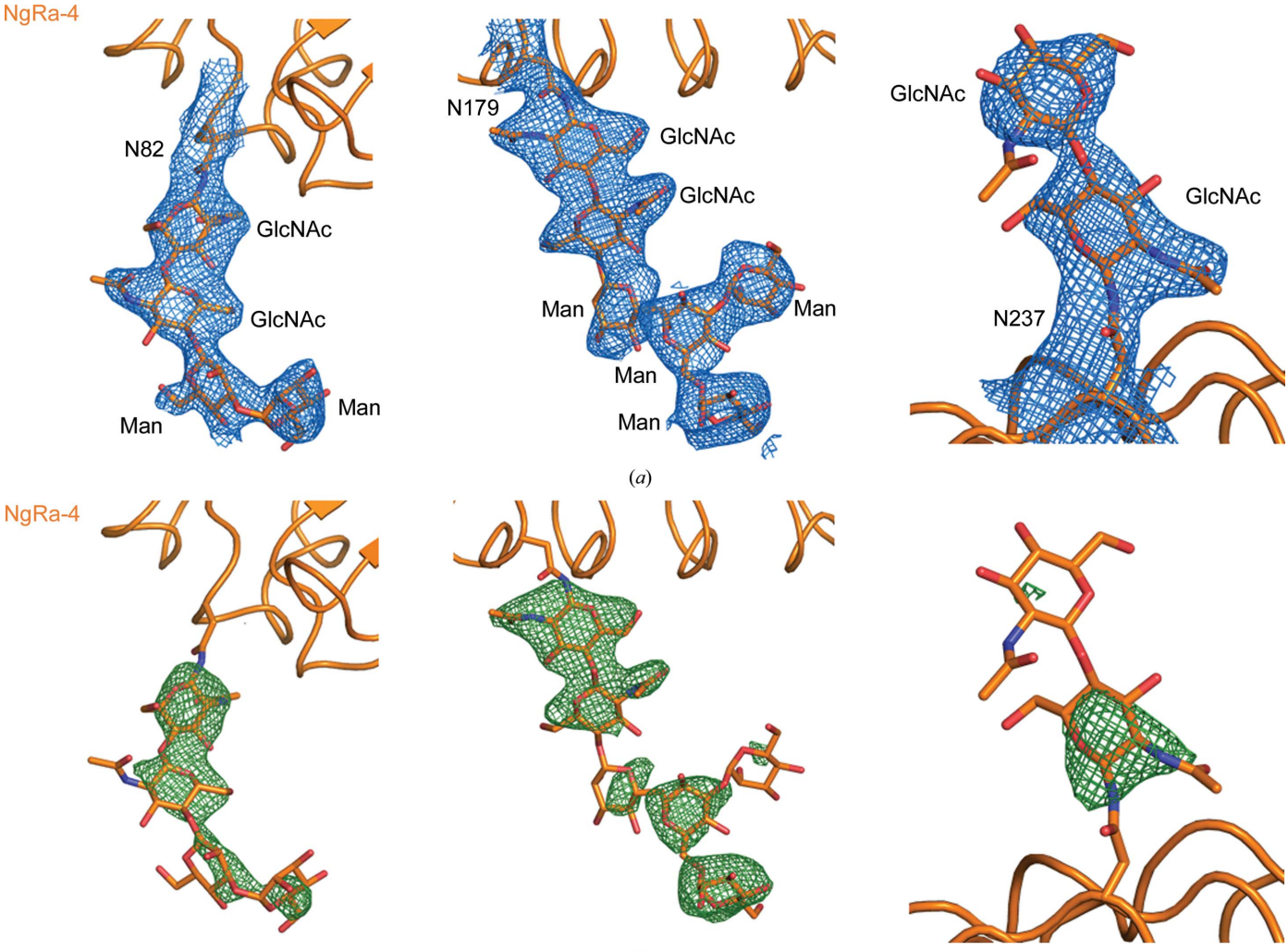

Figure 3
Electron density for the N-linked glycans on the NgR LRR. (*a*) $2F_o - F_c$ electron density for the glycosylated NgRa-4 crystal form at a contour level of 1.0σ around the N-linked glycans on Asn82 (left panel), Asn179 (middle panel) and Asn237 (right panel), confirming the previously confirmed glycosylation sites on Asn82 and Asn179 (He *et al.*, 2003) and showing clear electron density for the N-linked glycosylation site at Asn237. (*b*) As in (*a*) but showing the $F_o - F_c$ simulated-annealing OMIT density (glycans omitted) at a contour level of 3.0σ for the same glycans.

the aforementioned mass-spectrometry study (Wen *et al.*, 2005) to form a disulfide with each other and are thus not expected to interfere with the disulfides in the construct used. The overall structure of the NgR LRR domain, including the C-terminal cap, is not affected by the artificial disulfide structure reported previously (Barton *et al.*, 2003; He *et al.*, 2003; Weinreb *et al.*, 2010) (Fig. 2*a*).

The C-terminal segment (residues 310–334) forms a loop in our structures. This loop is disordered in most of the structures despite being anchored to the C-terminal cap by two disulfides: Cys266–Cys335 and Cys309–Cys336. Only in one crystal form, NgRa-5, could the entire loop be modelled in the electron density. In this crystal form, eight NgRa molecules are present in the asymmetric unit, related by point-group 422 noncrystallographic symmetry. For these NgRa molecules, a relatively large portion of the loop is observed in the electron density (Fig. 2*b*). For one of the NgRa molecules in the NgRa-5 crystal form (called chain *B*) the whole loop could be modelled, albeit in relatively weak electron density with high isotropic displacement parameters (IDPs), in particular for residues 313–318 (Figs. 2*c*, 2*d* and 2*e*). The loop is also relatively well resolved in the NgRa-4 crystal form (except for residues 317–321), likely owing to stabilizing packing interactions. In this crystal form, the loop adopts a conformation similar to that in the NgRa-5 crystal form (Fig. 2*b*). In both NgRa-4 and NgRa-5, α-helical secondary structure can be observed in the C-terminal segment and the C-terminus (residues C-terminal of Cys336). The α-helix in the C-terminal segment may represent a native structure. The α-helix observed at the C-terminus, on the other hand, is most likely to be an artifact, since most residues in this segment (QAAAHH) are part of the cloning-restriction site and purification tag (AAAHHHHHH). In the full-length protein and in the NgRb construct a proline is present in this segment instead of the first alanine (Pro338; Fig. 1) that likely perturbs the α-helix (Yun *et al.*, 1991). Indeed, no α-helical structure is observed for the C-terminus in any of the NgRb structures. The fragments of loop 310–334 that are observed in the electron density of crystal forms other than NgRa-4 and NgRa-5 are structurally heterogeneous (Fig. 2*a*). Concluding, the fragmented or absent electron density, the high IDPs and the heterogeneous conformations of the C-terminal segment in the different crystal forms indicate that it is a flexible loop in the absence of stabilizing interactions (Fig. 2). Nonetheless, a preference for a possibly energetically

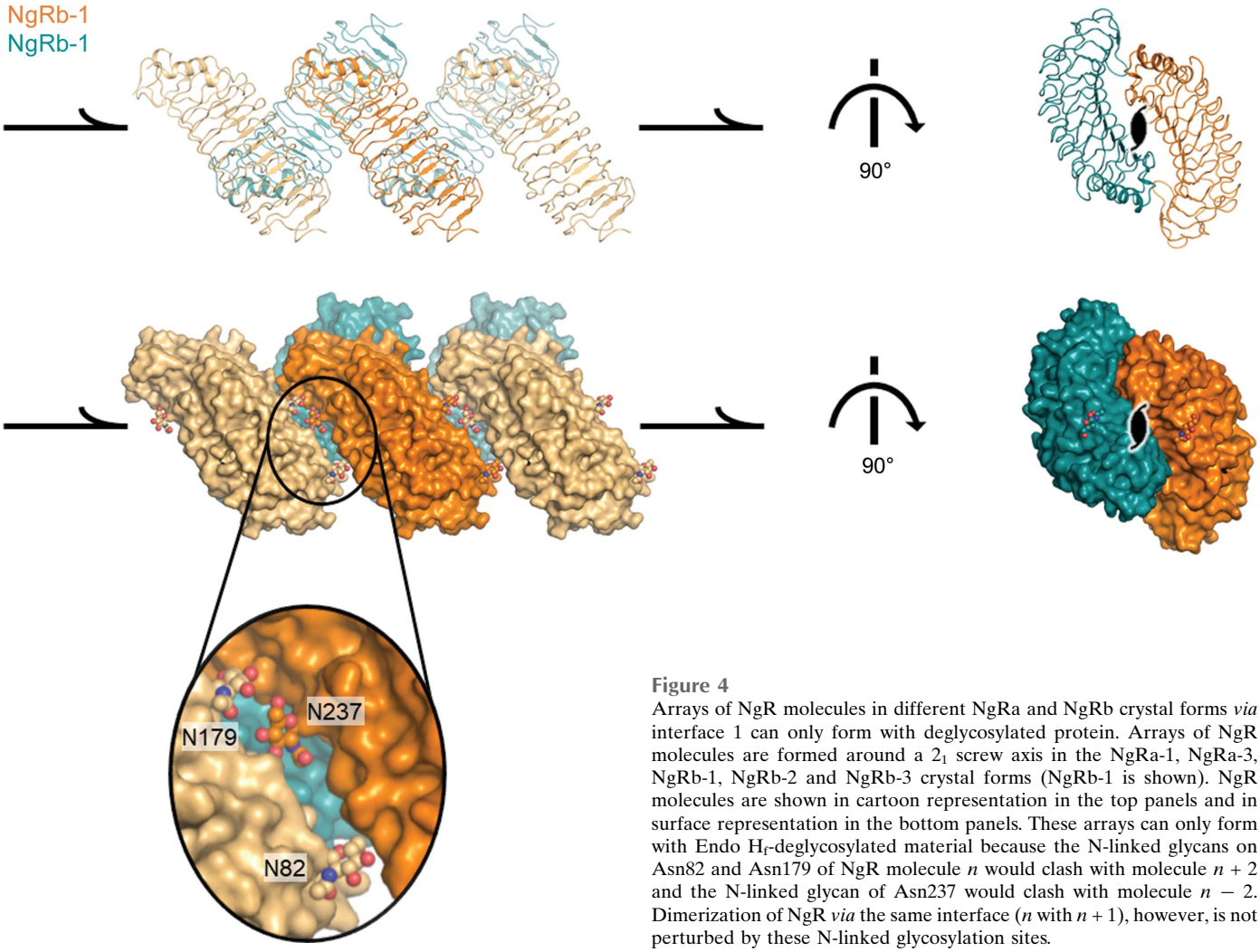

Figure 4
Arrays of NgR molecules in different NgRa and NgRb crystal forms *via* interface 1 can only form with deglycosylated protein. Arrays of NgR molecules are formed around a 2_1 screw axis in the NgRa-1, NgRa-3, NgRb-1, NgRb-2 and NgRb-3 crystal forms (NgRb-1 is shown). NgR molecules are shown in cartoon representation in the top panels and in surface representation in the bottom panels. These arrays can only form with Endo H_f-deglycosylated material because the N-linked glycans on Asn82 and Asn179 of NgR molecule n would clash with molecule $n + 2$ and the N-linked glycan of Asn237 would clash with molecule $n - 2$. Dimerization of NgR *via* the same interface (n with $n + 1$), however, is not perturbed by these N-linked glycosylation sites.

favoured conformation of this C-terminal loop is suggested by its similar structure in the unrelated NgRa-4 and NgRa-5 crystal forms.

3.2. NgR self-associates in different crystal forms through a shared interface

Since NgR was previously shown to self-interact on a cell surface, we analyzed the crystal-packing interfaces of all of our NgR structures as well as those previously solved by others (Barton *et al.*, 2003; He *et al.*, 2003; Weinreb *et al.*, 2010). Remarkably, several different crystal forms of both NgRa and NgRb share a crystal-packing interface involving the concave surface of the NgR LRR (NgRa-1, NgRa-3, NgRb-1, NgRb-2 and NgRb-3), hereafter referred to as interface 1.

The crystals in which NgR packs *via* interface 1 all grew in conditions buffered at pH 5 (Table 3). Interface 1 is part of linear arrays of interacting NgR molecules along a 2_1 screw axis with a pitch of 46.6 ± 0.3 Å (Fig. 4). In some crystal forms, this is a crystallographic screw axis (NgRa-3, NgRb-2 and NgRb-3; space groups $P2_12_12_1$, $P2_1$ and $P2_12_12_1$, respectively). In the crystal forms with space group $C2$ (NgRa-1 and NgRb-1) the same interface is formed by the combination of a crystallographic twofold rotation and translation along the *b* axis of one unit cell. In these crystal forms, the *b* axis has a dimension of 46.6 Å (see Table 2), equivalent to the pitch of the screw axis in NgRa-3, NgRb-2 and NgRb-3. All crystals that showed such NgR arrays had needle-like macroscopic morphology and *vice versa*, suggesting that the screw axes of NgR arrays correspond to the long axes of the needle crystals. However, these arrays are only observed in Endo H_f-deglycosylated crystal forms and cannot form with native glycosylated NgR, although dimerization *via* interface 1 is still possible (Fig. 4). N-linked glycans on Asn82 and Asn179 of NgR molecule *n* would clash with the LRR of NgR molecule *n* + 2. Similarly, the N-linked glycan on Asn237 of NgR molecule *n* would clash with the LRR of NgR molecule *n* − 2. However, these glycans do not interfere with dimerization *via* interface 1 (*n* with *n* + 1) as observed in these crystals (Fig. 4). Thus, for natively glycosylated NgR dimers should still be able to form *via* interface 1, whereas further multimerization would be blocked by the three N-linked glycans on the NgR LRR.

Interface 1 is mostly hydrophilic and has an interface area of approximately 750 Å^2. The N-terminal LRR cap and concave

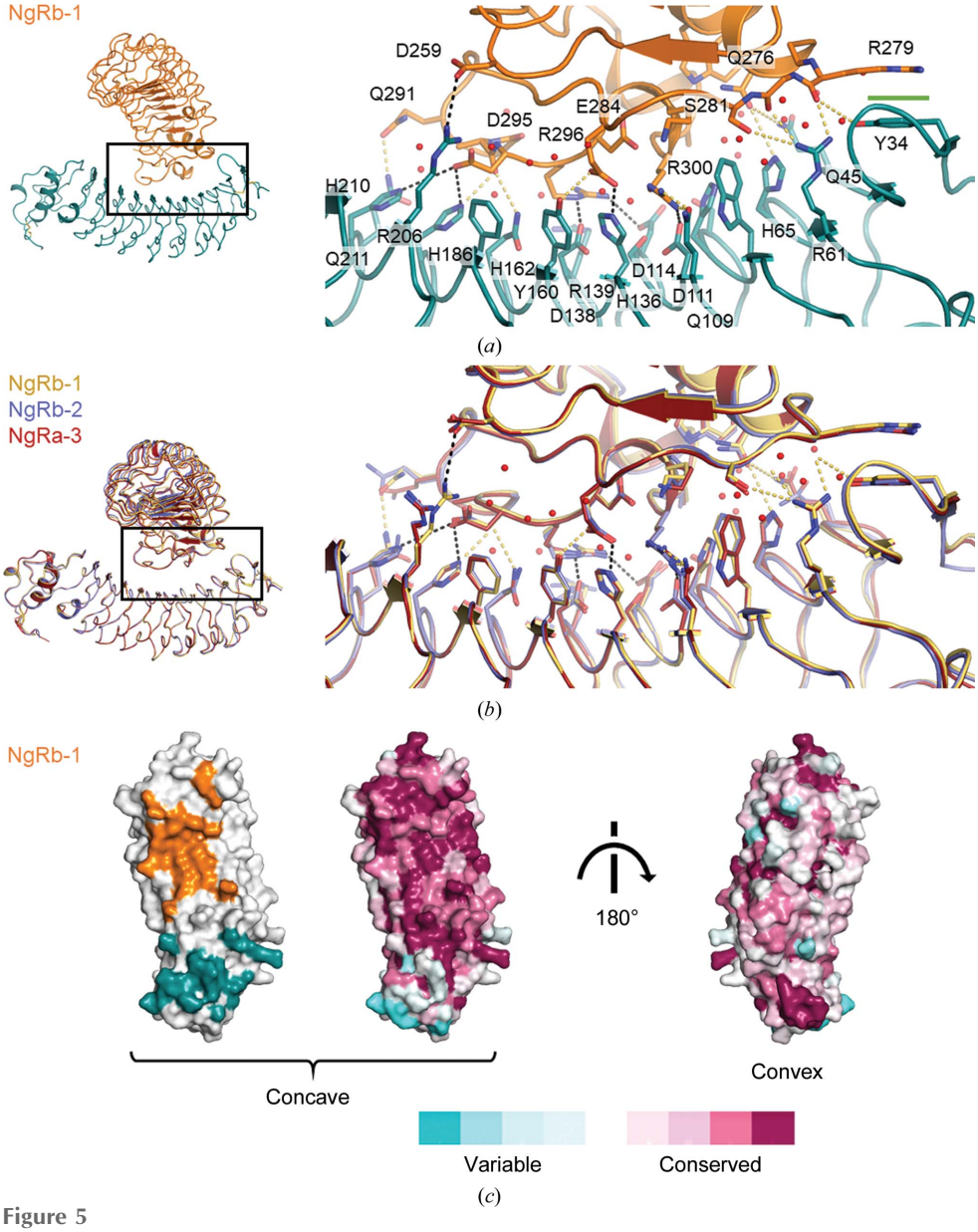

Figure 5
Analysis of interface 1. (*a*) Close-up view of interface 1. Salt bridges are indicated by black dashed lines, direct hydrogen bonds by yellow dashed lines and the π–π interaction between Arg279 and Tyr34 by a green rectangle. Residues at the interface are shown in stick representation and those involved in intermolecular interactions are additionally labelled; other residues at the interface are also shown as sticks. Red spheres represent ordered solvent molecules near the interface. (*b*) The same representation as in (*a*), comparing the independent crystal forms of NgRb-1, NgRb-2 and NgRa-3 that share this interface. These crystal forms have highly similar orientations of the amino-acid side chains involved in the formation of this interface. (*c*) Footprints of the interface [left panel; colouring as in (*a*)] and evolutionary conservation of the surface residues (right panels; purple is more conserved, cyan is less conserved).

	Interface 1 (Fig. 5)	NgRa-2 (Fig. 7*b*)	1ozn (Figs. 6*a* and 6*b*)
Surface area (Å^2)	750	660	860
pH of crystallization condition	5	4	6.5
Predicted ΔG (kcal mol^{-1}) (Vangone & Bonvin, 2015)	−9.8	−8.2	−7.5
Interface contacts	Asp111–Arg300	Arg300–Asp163	Arg131–Asp114
	Asp114–Arg296	Arg256–Asp259	Asn176–Arg189
	His136–Glu284	Arg206–Glu284	His202–Asp259
	Asp138–Arg296	His186–Asp295	Arg227–Asp259
	Arg206–Asp259	Ser282*–Gln211	Arg250–Glu284
	His186–Asp295	Tyr254–Asp259	Thr243–Gln291
	His210–Asp295	Tyr232–Asp259	GlcNAc2 on Asn82–Gln46
	Tyr34–Arg279	Arg139–Gln291	
	Gln45–Gln276		
	Arg61–Arg279*		
	Arg61–Gly280*		
	Arg61–Ser281		
	His65–Gln276		
	Gln109–Arg300		
	Gln162–Ala294*		
	His186–Ala294*		
	Gln211–Gln291		
	Tyr160–Glu284		

Figure 6
Comparison of relevant crystal-packing interfaces. Asterisks indicate hydrogen bonds to backbone carbonyls. Salt bridges are coloured blue, π–π interactions green and hydrogen bonds yellow.

side of one NgR LRR (the interface spans LRRs 1–7) interacts with the concave face of the C-terminal LRR cap of another NgR molecule (Fig. 5*a*). The interaction is stabilized by seven salt bridges, ten direct hydrogen bonds and a π–π interaction between the side chains of Tyr34 and Arg279 (see Figs. 5*a*, 6 and 7*b*). Three salt bridges are formed by a histidine paired with a negatively charged amino acid (His136–Glu284, His210–Asp295 and His186–Asp295). This suggests that this interaction could be pH-regulated, since histidine side chains are only positively charged at lower pH values owing to the pK_a values of their side chains being approximately 5.5–7.0, depending on the local chemical environment (Bradbury & Scheraga, 1966; Markley, 1975). Apart from the ten direct hydrogen bonds, several indirect hydrogen bonds are formed *via* ordered water molecules at the interface. As has previously been shown by others (He *et al.*, 2003), the concave surface of the NgR LRR is also evolutionarily conserved compared with the convex surface (Fig. 5*c*).

3.3. Other crystallographic interfaces observed for NgR are less extensive

Some other crystal forms also have substantial packing interfaces (Fig. 6). Both previously published structures (PDB entries 1ozn and 1p8t) have interfaces with surface areas of >750 Å^2. The 1ozn structure has extended crystal-packing interfaces on the sides of the LRR domains that would result in parallel arrays (Fig. 7*a*). This interface has a surface area of 860 Å^2 and is stabilized by five salt bridges and two direct hydrogen bonds. The N-linked glycans on Asn82 and Asn179 also contribute to this interface (Fig. 7*a*). However, these side faces of the LRR are evolutionarily not as conserved (Fig. 7*b*) compared with the concave surface of the LRR (Fig. 5*c*). In the paper describing 1ozn, another interface is suggested for NgR self-interaction (He *et al.*, 2003). However, this interface would not be possible for NgR with its native disulfide structure because of steric hindrance (Fig. 7*c*). In the 1p8t structure (Barton *et al.*, 2003) the largest interface has a surface area of 790 Å^2 and is stabilized by one salt bridge and five direct hydrogen bonds, as well as some hydrophobic contacts (Fig. 8*a*). This interface is formed by the bottom side of the C-terminal LRR cap of one molecule of NgR binding to the N-terminal LRR capping domain and five LRRs of another NgR molecule. However, this interface relies on interactions of the artificial disulfide Cys266–Cys309 and the C-terminus and is thus not likely to be formed in full-length NgR (Fig. 8*a*).

The NgRa-2 crystal form also has a significant unique interface between two NgR monomers in the asymmetric unit oriented in an asymmetric antiparallel fashion (Fig. 8*b*). This hydrophilic interface has a surface area of 660 Å^2 and is stabilized by four intermolecular salt bridges and four hydrogen bonds. It involves the evolutionarily conserved concave surface of NgR and is also stabilized by a salt bridge between a histidine (His186) and an aspartate (Asp295) (Fig. 8*b*). The NgRa-2 crystal was grown at the lowest pH condition compared with the other crystal forms (pH 4.0; see Table 3). All other interfaces were too small or improbable to consider and will not be discussed here.

3.4. NgR self-interaction analyzed in solution

To delineate which of the aforementioned interfaces is relevant in solution, site-directed mutagenesis was combined with biophysical solution-state techniques. Charge-swap mutations of two residues involved in salt bridges in different interfaces were introduced into the NgRb construct: D111R and R300E (see Figs. 2 and 6). Both mutants interfere with salt bridges formed at interface 1, whereas only R300E would interfere with a salt bridge in the NgRa-2 interface (Figs. 5*a*, 6 and 8*b*). Based on the structure, neither mutant should interfere with the array-forming interface in the 1ozn crystal form (Figs. 6 and 7*a*).

Small-angle X-ray scattering (SAXS) was used to analyze the solution behaviour of wild-type NgR LRR and mutants. As expected based on previous (cell-based) studies (Fournier *et al.*, 2002; Saha *et al.*, 2011; Barton *et al.*, 2003), both NgRa and NgRb wt self-associate in solution, as shown by the concentration-dependent increase of the size-dependent parameters radius of gyration (R_g), molecular mass (M_m) based on the scattering at zero scattering angle (I_0), peak shift

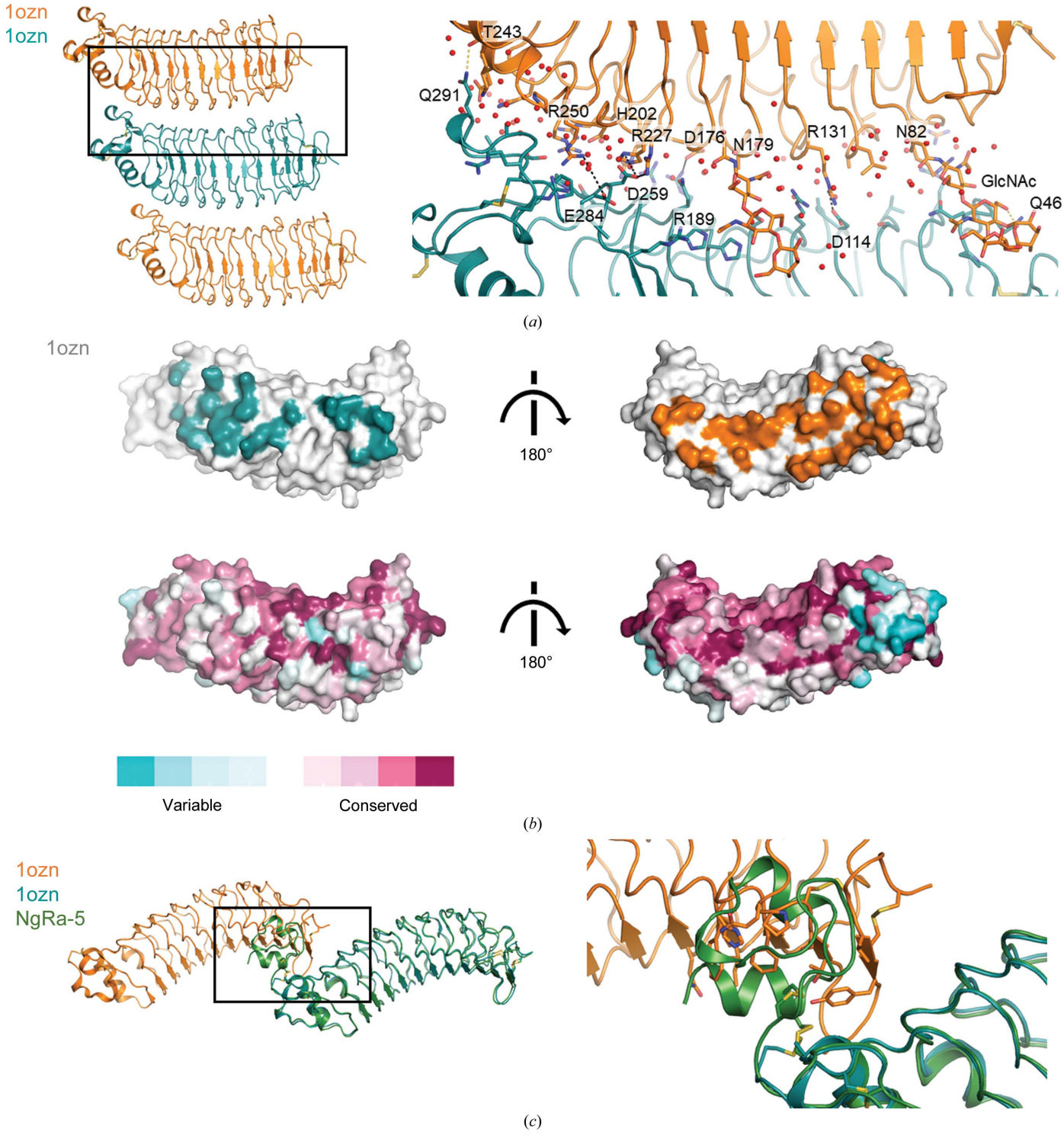

Figure 7
Analysis of interfaces for PDB entry 1ozn. (*a*) Close-up view of the linear array-forming interface in PDB entry 1ozn (He *et al.*, 2003) shown in the same representation as in Fig. 5. N-linked glycans on Asn82 and Asn179 are shown as sticks. (*b*) Footprints of the interface [top panels, colouring as in (*a*)] and evolutionary conservation of the surface residues (right panels; purple is more conserved, cyan is less conserved). (*c*) The interface in PDB entry 1ozn (orange and teal) that was suggested in the accompanying paper to represent the self-interaction of NgR (He *et al.*, 2003) cannot be formed if NgR has the correct disulfide pattern because of steric hindrance. The structure of NgRa-5 chain *B* is overlaid in green to indicate the clashes.

to larger distances in the paired-distance distribution, maximum dimension based on the paired-distance distribution function (D_{max}) and Porod volume (Table 1, Figs. 9 and 10). As a reference for monomeric protein, we used size-exclusion chromatography (SEC) coupled online to the SAXS cuvette for glycosylated NgRb. The R_g, D_{max} and Porod volume appear similar to those for our lower concentration samples of glycosylated NgRb, which presumably are also monomeric (Table 1).

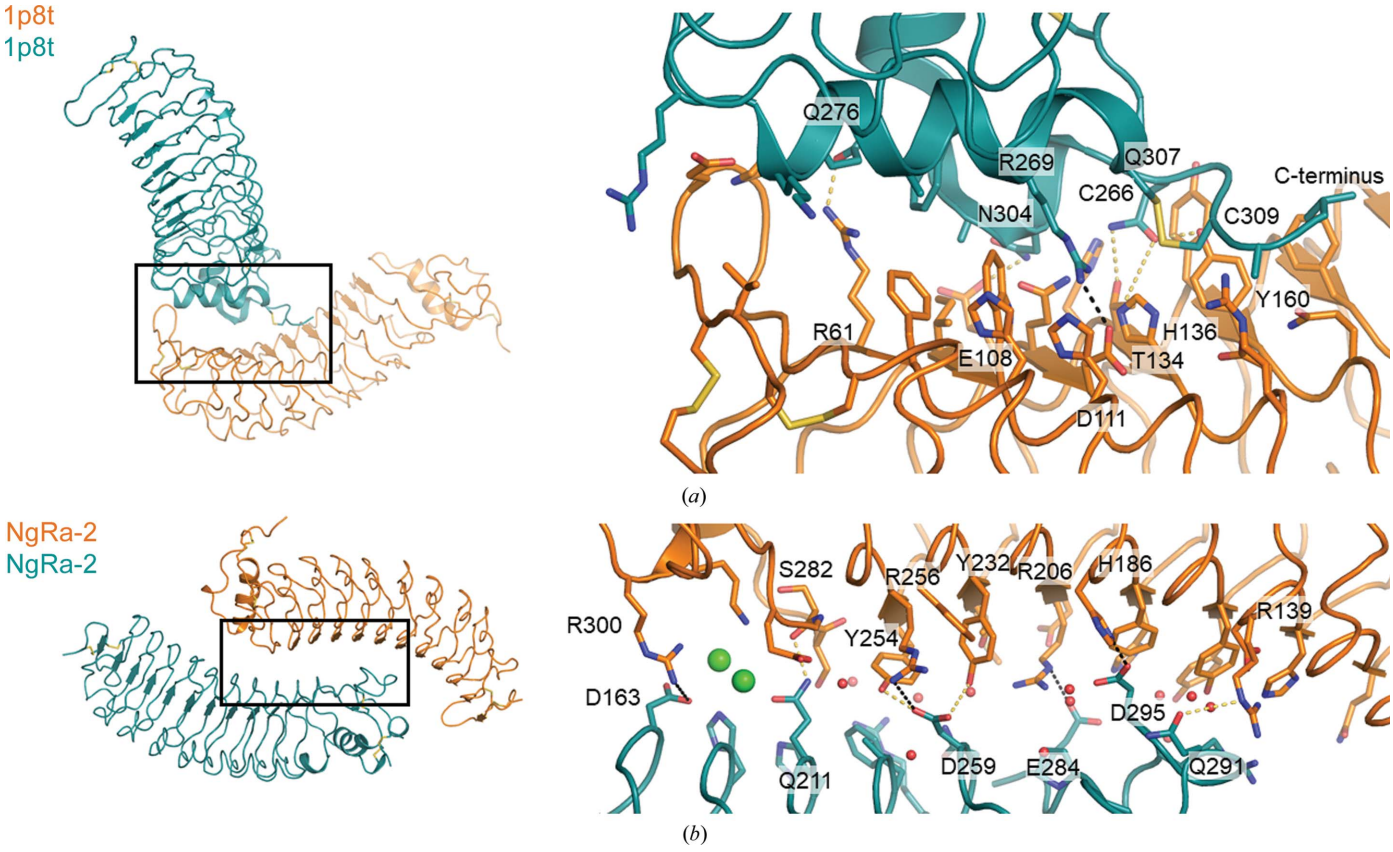

Figure 8
Other crystal-packing interfaces that might account for NgR self-interaction. (*a*) The largest interface in PDB entry 1p8t (Barton *et al.*, 2003) shown in the same representation as in Fig. 5. This interface appears to be mostly hydrophobic and is stabilized by the artificial disulfide Cys266–Cys309 and the C-terminus. (*b*) View of the interface between two monomers in the asymmetric unit of the NgRa-2 crystal form shown in the same representation as Fig. 5; green spheres represent chloride ions. These crystals appeared in a condition buffered at pH 4.

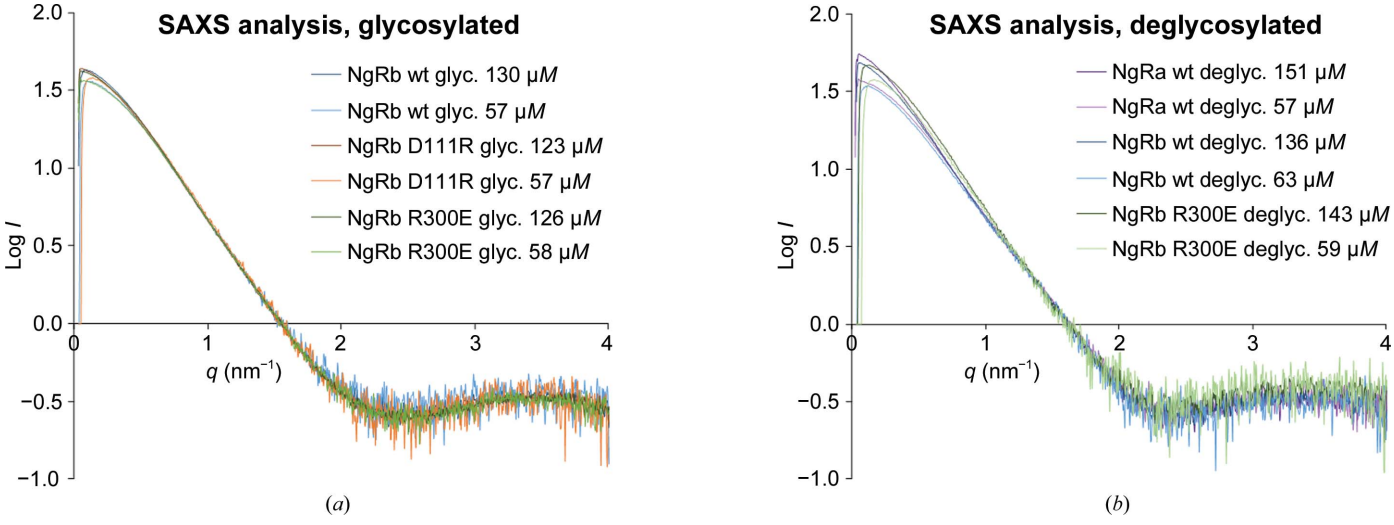

Figure 9
Small-angle X-ray scattering analysis of NgR constructs in solution. Small-angle X-ray scattering log *I versus q* plots of glycosylated (*a*) and deglycosylated (*b*) NgR constructs (see also Table 1).

We observe a stronger concentration-dependent self-association for deglycosylated NgRb and NgRa wt compared with glycosylated NgRb wt (Figs. 9 and 10). This is in agreement with interface 1 being the predominant self-association interface in solution. As discussed previously, this interface would only tolerate dimerization for glycosylated material, whereas Endo H_f-deglycosylated NgR could form multimeric arrays (see Fig. 4). The arrays observed for the 1ozn structure, on the other hand, appear to be stabilized by the N-linked glycans (Fig. 7*a*), which is in conflict with the trends that we observe in the size-dependent SAXS parameters for Endo H_f-deglycosylated protein compared with glycosylated protein. Thus, our data for wild-type NgRa and NgRb indicate that the LRR domain of NgR is sufficient for self-association, as observed on cells (Fournier *et al.*, 2002; Barton *et al.*, 2003), and the more pronounced concentration-dependent self-association for deglycosylated NgR suggest interface 1, rather than the array-forming interface observed for the 1ozn structure, to be responsible for this self-association.

However, we did not observe notable differences in the aforementioned SAXS-derived size-dependent parameters when comparing the wild-type protein with our D111R and R300E mutants that should, based on our structures, disrupt interface 1 (Table 1, Figs. 9 and 10). Although for the

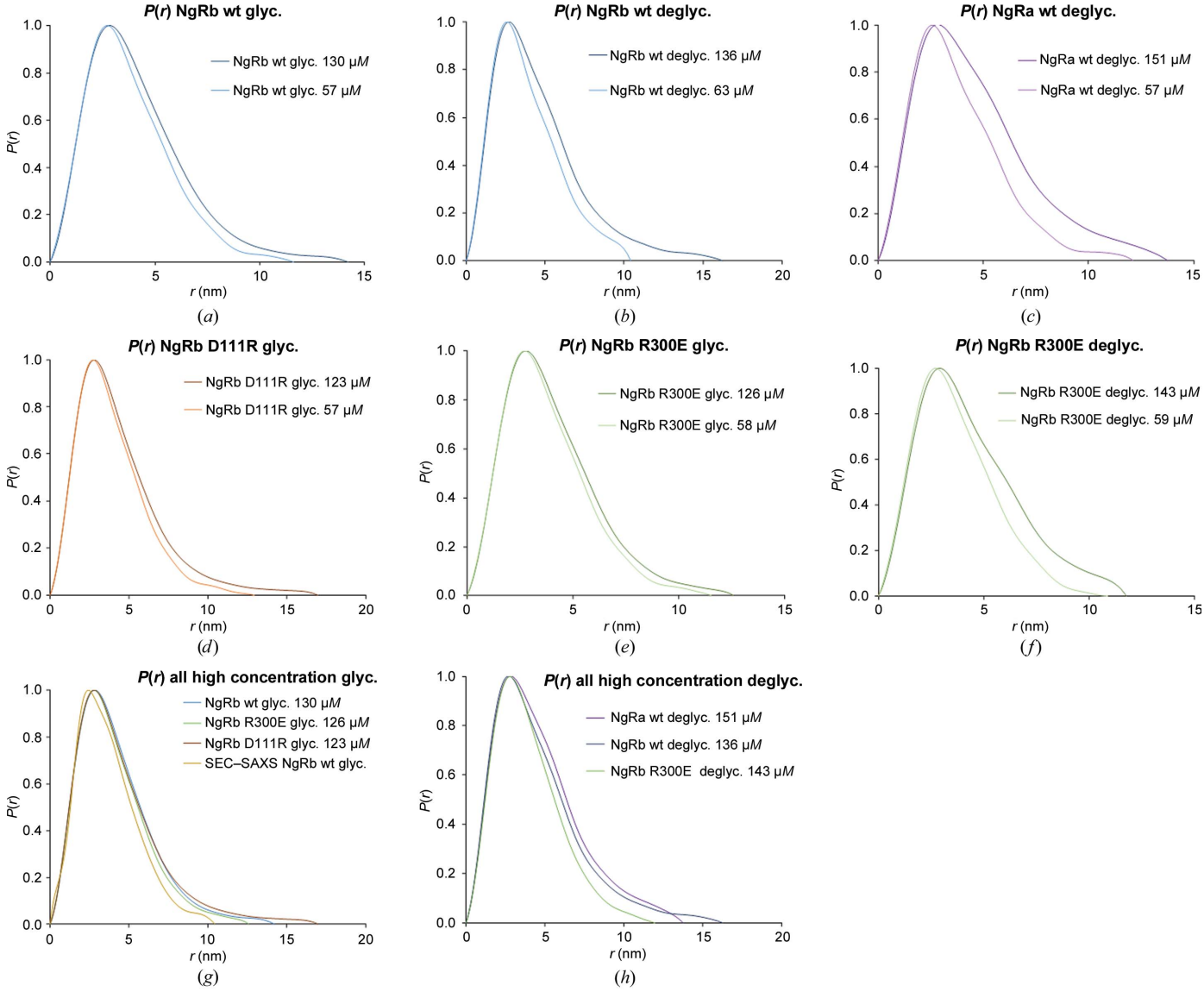

Figure 10
SAXS-derived paired distance distribution functions suggest that the NgR LRR self-associates. (*a*) The SAXS-derived paired distance distribution function $P(r)$ for glycosylated NgRb wt at different concentrations shows concentration-dependent self-association. (*b*) Deglycosylated NgRb wt shows stronger concentration-dependent self-association than NgRb wt (*a*). (*c*) Concentration-dependent self-association of deglycosylated NgRa wt is even more pronounced than for NgRb (*b*). (*d*) $P(r)$ for glycosylated NgRb D111R mutant shows a very modest self-association. (*e*) $P(r)$ for glycosylated NgRb R300E shows slightly stronger self-association than NgRb D111R. (*f*) Deglycosylated NgRb R300E shows a stronger self-association than glycosylated NgRb R300E. (*g*) Comparing all glycosylated variants at the highest concentration, no clear difference could be seen between the wild type and mutants. However, the paired distance distributions of these samples do all represent an ensemble of (on average) larger particles than that of monomeric NgRb obtained from SEC–SAXS measurements. (*h*) The deglycosylated wild-type NgRa and NgRb appear to be larger than the deglycosylated NgRb R300E mutant at the highest concentrations.

deglycosylated NgRb R300E mutant there is a clear difference in R_g and D_{max}, with larger values compared with NgRa or NgRb wt, the differences in Porod volume and M_m based on the I_0 are negligible (Table 1, Figs. 9 and 10). For the glycosylated mutants, the difference in all size-dependent SAXS parameters from the wild type is negligible, whereas a clear concentration-dependence remained observable. This implies that either the mutants do not sufficiently disrupt self-association *via* interface 1 or that another interface is (partly) responsible for the observed self-association.

To further investigate NgR self-association, we performed sedimentation-velocity analytical ultracentrifugation (SV-AUC) experiments with glycosylated NgRb wt, D111R and R300E. The samples were diluted to have the same starting concentration of 95 µ*M*. A clear difference in sedimentation coefficient could be observed on comparing the wild type and mutants (Fig. 11). While a shifted and broader peak and shoulder at higher sedimentation coefficients could be observed for the wild type, suggesting monomer–dimer exchange, the D111R mutant showed a single species with a smaller sedimentation coefficient. The R300E mutant appeared to be somewhat larger and broader than the D111R mutant, reminiscent of the main species observed for the wild type. However, the shoulder at a larger sedimentation coefficient was not observed for this mutant. Thus, the SV-AUC experiments indicate that monomer–dimer exchange occurs for wild-type glycosylated NgRb at the concentration used. For the R300E mutant and especially the D111R mutant, on the other hand, this effect is less pronounced, suggesting that these mutants do, to some extent, interfere with NgR self-interaction.

4. Discussion

Our structures indicate that the overall structure of the NgR LRR and the C-terminal cap is not altered by the non-native disulfide structure present in the previously published NgR structures (Barton *et al.*, 2003; He *et al.*, 2003; Fig. 2*a*). An extra C-terminal loop is formed by the disulfides Cys266–Cys335 and Cys309–Cys336. This C-terminal loop appears to be flexible in the absence of any stabilizing interactions. We could model (part of) this loop in two independent crystal forms, which reveals a similar yet flexible structure (Fig. 2*b*). The structure of the C-terminal loop in these two crystal forms deviates from a previously proposed model in which this loop was proposed to fold back to the convex side of the NgR LRR (Wen *et al.*, 2005). This loop is not required for MAI ligand binding (Wang, Koprivica *et al.*, 2002; Liu *et al.*, 2002; Fournier *et al.*, 2002; Barton *et al.*, 2003; Venkatesh *et al.*, 2005; Laurén *et al.*, 2007; Robak *et al.*, 2009), but previous work shows that it contributes to the interaction with the co-receptors p75 and TROY (Shao *et al.*, 2005). Structures of NgR–p75 or NgR–TROY complexes are required to determine whether the C-terminal loop indeed adopts a defined structure when interacting with these co-receptors.

To investigate the structural basis of the previously described NgR self-interaction (Fournier *et al.*, 2002; Saha *et al.*, 2011; Barton *et al.*, 2003), we compared the crystallographic interfaces in six new unique crystal forms of NgRa and NgRb, as well as those of the two previously published structures [PDB entries 1p8t (Barton *et al.*, 2003) and 1ozn (He *et al.*, 2003)]. We identified extensive interfaces in the NgRa and NgRb structures, most notably interface 1 found in five of our structures (NgRa-1, NgRa-3, NgRb-1, NgRb-2 and NgRb-3) encompassing three independent crystal forms (space groups $C2$, $P2_1$ and $P2_12_12_1$). This interface has more inter-protein salt bridges (seven) and hydrogen bonds (ten) than any of the other interfaces and is predicted by the *PRODIGY* server (Vangone & Bonvin, 2015) to be the most energetically favourable (Fig. 6). Moreover, it is the only interface found in more than one crystallization condition (five out of ten in total, eight of which are described here and two previously published; Barton *et al.*, 2003; He *et al.*, 2003). Several other interfaces have larger surface areas, but are not stabilized by as many contacts (Fig. 6). Some of these can only be formed for NgR constructs with the artificial disulfide pattern in the C-terminal cap (interfaces in PDB entries 1ozn and 1p8t; see Figs. 7*c* and 8*a*, respectively). The remaining candidate interfaces have fewer inter-protein salt bridges and hydrogen bonds while not being hydrophobic either (the other interface in 1ozn and the NgRa-2 interface; see Fig. 6), are formed *via* nonconserved interfaces (interface in 1ozn; see Fig. 6*b*) or are formed at pH 4 (interface in NgRa-2). This prompted us to further probe the importance of interface 1 in NgR self-association.

Our biophysical analysis of purified NgRa and NgRb in solution by SAXS and SV-AUC does not unambiguously define the NgR self-association-determining interface. Our SAXS data show a clear concentration-dependent self-association for both glycosylated and deglycosylated NgR

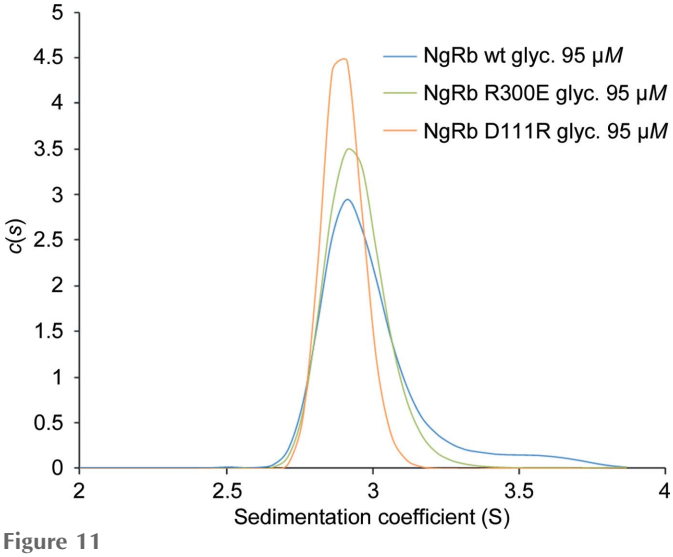

Figure 11
Sedimentation-velocity analytical ultracentrifugation analysis of NgRb wt and mutants. In SV-AUC experiments, no convincing dimer peak could be observed. However, a clear shift and shoulder towards larger species is observed for NgRb wt compared with the D111R and R300E mutants, suggesting monomer–dimer exchange during the experiment for NgRb wt.

constructs, confirming the previously demonstrated NgR self-interaction (Fournier *et al.*, 2002; Saha *et al.*, 2011; Barton *et al.*, 2003). Furthermore, the stronger concentration-dependence for deglycosylated NgRb compared with glycosylated NgRb suggests interface 1, rather than the array-forming interface of the 1ozn crystal form, to represent NgRb self-interaction in solution. However, our structure-guided mutations did not significantly interfere with dimer formation in our SAXS analysis. In the SV-AUC experiments there was an observable difference for the three samples, but it was rather subtle. Possibly, these mutants do not strongly interfere with complex formation *via* interface 1, as only a single salt bridge of the seven in total is reversed. Alternatively, these observations could be explained by the array-forming interface of PDB entry 1ozn being predominant in solution. However, in this case one would expect stronger self-interaction, rather than weaker, for glycosylated compared with deglycosylated NgRb (Fig. 7*a*).

Although eight independent crystal forms of NgR are now available, there is still a possibility that NgR self-interaction is not represented in any of these crystal forms. This is, however, unlikely as NgR was crystallized at high concentrations of 250–350 μ*M*. Therefore, we argue that interaction *via* interface 1 is most likely to represent the previously reported NgR self-interaction (Fournier *et al.*, 2002; Saha *et al.*, 2011; Barton *et al.*, 2003). The flexible glycosylated stalk of NgR should allow two NgR LRRs to interact in this fashion on a cell surface *in cis* (Fournier *et al.*, 2002).

Interestingly, NgR self-association *via* interface 1 might be pH-controlled, as three of the seven intermolecular salt bridges are formed between the side chains of pH-sensitive histidine residues (Bradbury & Scheraga, 1966; Markley, 1975) and negatively charged amino acids (aspartate and glutamate) (Fig. 6). Moreover, these crystals all appeared at pH 5 (Table 3), indicating that this interface is likely to be more stable at lower pH. Possibly, this could play a role during trafficking of NgR through the secretory pathway or upon internalization, as low pH values occur in both secretory and endosomal compartments (Demaurex, 2002). Ligand-induced internalization has been suggested previously (Meabon *et al.*, 2015) and could occur upon the binding of cell-surface-shed MAI ligands such as dMAG (Tang *et al.*, 1997). The two previously published structures were both crystallized at pH 6.5 (Barton *et al.*, 2003; He *et al.*, 2003), similar to our NgRa-4 crystal form (Table 3 and Fig. 6). These three crystal forms have no crystal-packing interfaces in common and the interfaces that are present are less extensive and less conserved than interface 1, as discussed above. This indicates that the interaction interfaces observed in these crystal forms are not likely to represent NgR self-interaction on the cell surface, in spite of their more neutral crystallization pH.

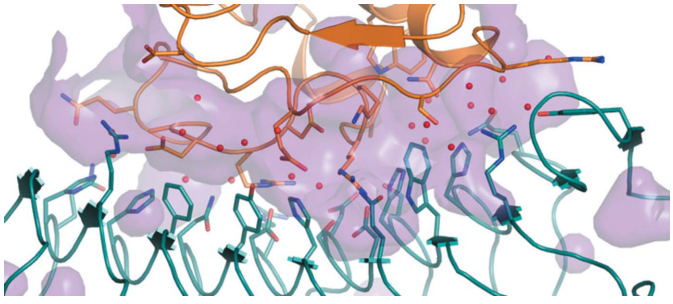

Figure 12
Cavity surface of interface 1. The interface is represented as in Fig. 5(*a*). The cavity formed in between the molecules is indicated by a purple surface. If this dimer, formed *via* interface 1, represents an inactive signalling form, these cavities could be exploited by designing dimer-stabilizing small molecules to antagonize MAI signalling and enhance regeneration upon CNS injury.

Interface 1 involves the concave side of one NgR LRR, whereas for the other NgR molecule in the dimer this concave LRR side remains available for interaction with other ligands (Fig. 5*a*). Previous work using scanning alanine mutagenesis of surface residues has shown that Nogo66, MAG and OMgp are most likely to bind to the concave side of the NgR LRR (Laurén *et al.*, 2007). In addition, the presence of glutathione *S*-transferase (GST)-linked Nogo66 did not strongly affect the ability of NgR to self-interact (Fournier *et al.*, 2002). Whether or not the NgR self-interaction *via* interface 1 is compatible with ligand binding needs further study.

NgR has been shown to preferentially bind to dimeric disulfide-linked p75 in a conformation with associating intracellular death domains, which is likely to represent the active MAI signalling state (Vilar *et al.*, 2014). These disulfide-linked p75 dimers have been proposed to transduce signalling through the membrane *via* scissoring mechanisms depending on extracellular ligand binding (Vilar, Charalampopoulos, Kenchappa, Simi *et al.*, 2009; Vilar, Charalampopoulos, Kenchappa, Reversi *et al.*, 2009; Vilar *et al.*, 2014). These results suggest that dimers of NgR can interact with dimeric p75, and depending on the three-dimensional arrangement of their extracellular domains such complexes could transmit different signals through the membrane. It is possible that NgR–p75 complexes can be in both active and inactive conformations, depending on the presence of the MAI ligand, as suggested previously (Barton *et al.*, 2003). Interestingly, inactive and active dimers have been reported for plexins (Kong *et al.*, 2016) and ephrin receptors (Himanen *et al.*, 2001), both of which are axon-guidance receptors that signal *via* RhoA/ROCK and inhibit CNS regeneration upon injury, similar to NgR (Pasterkamp *et al.*, 2001; Benson *et al.*, 2005; Bolsover *et al.*, 2008; Kolodkin & Tessier-Lavigne, 2011). Further investigation is required to determine whether NgR dimers formed *via* interface 1 represent an active or an inactive signalling state.

If the dimer that forms *via* interface 1 represents an inactive signalling state, this could be a target for pharmacological intervention with small-molecule therapeutics. These dimers have significant cavities in between the two monomers that could be exploited by dimer-stabilizing small molecules that keep NgR in a silent signalling state even in the presence of MAIs (Fig. 12). Conversely, if interface 1 represents an active signalling state, small molecules could be designed that interfere with the formation of the protein–protein interaction interface that we report.

Acknowledgements

We thank Dominique Thies-Weesie for assistance in setting up and analyzing the SV-AUC experiment. We thank the staff of the European Synchrotron Radiation Facility (ESRF) beamlines ID23-1, ID23-2 and ID29 and Swiss Light Source (SLS) beamline X06SA for assistance with diffraction data collection and the staff of ESRF beamline BM29 for assistance with SAXS data collection. MFP and BJCJ designed the experiments. MFP generated the constructs, purified the proteins, performed crystallization and solved and refined the structures, and performed SAXS and SV-AUC experiments and data analysis. RJT, HCV and MFP purified the proteins and set up the crystallization experiments that resulted in the NgRa-4 structure. BJCJ supervised the project. MFP and BJCJ wrote the manuscript with input from all authors.

Funding information

This work was funded by a Vidi grant (723.012.002) from the Netherlands Organization for Scientific Research to BJCJ.

References

Afonine, P. V., Grosse-Kunstleve, R. W., Echols, N., Headd, J. J., Moriarty, N. W., Mustyakimov, M., Terwilliger, T. C., Urzhumtsev, A., Zwart, P. H. & Adams, P. D. (2012). *Acta Cryst.* D**68**, 352–367.
Akbik, F. V., Bhagat, S. M., Patel, P. R., Cafferty, W. B. J. & Strittmatter, S. M. (2013). *Neuron*, **77**, 859–866.
Akbik, F., Cafferty, W. B. J. & Strittmatter, S. M. (2012). *Exp. Neurol.* **235**, 43–52.
Baldwin, K. T. & Giger, R. J. (2015). *Front. Mol. Neurosci.* **8**, 23.
Barton, W. A., Liu, B. P., Tzvetkova, D., Jeffrey, P. D., Fournier, A. E., Sah, D., Cate, R., Strittmatter, S. M. & Nikolov, D. B. (2003). *EMBO J.* **22**, 3291–3302.
Battye, T. G. G., Kontogiannis, L., Johnson, O., Powell, H. R. & Leslie, A. G. W. (2011). *Acta Cryst.* D**67**, 271–281.
Benson, M. D., Romero, M. I., Lush, M. E., Lu, Q. R., Henkemeyer, M. & Parada, L. F. (2005). *Proc. Natl Acad. Sci. USA*, **102**, 10694–10699.
Bolsover, S., Fabes, J. & Anderson, P. N. (2008). *Restor. Neurol. Neurosci.* **26**, 117–130.
Bradbury, J. H. & Scheraga, H. A. (1966). *J. Am. Chem. Soc.* **88**, 4240–4246.
Brown, P. H. & Schuck, P. (2006). *Biophys. J.* **90**, 4651–4661.
Demaurex, N. (2002). *News Physiol. Sci.* **17**, 1–5.
Emsley, P. & Cowtan, K. (2004). *Acta Cryst.* D**60**, 2126–2132.
Evans, P. R. (2011). *Acta Cryst.* D**67**, 282–292.
Evans, P. R. & Murshudov, G. N. (2013). *Acta Cryst.* D**69**, 1204–1214.
Fournier, A. E., Gould, G. C., Liu, B. P. & Strittmatter, S. M. (2002). *J. Neurosci.* **22**, 8876–8883.
Franke, D., Petoukhov, M. V., Konarev, P. V., Panjkovich, A., Tuukkanen, A., Mertens, H. D. T., Kikhney, A. G., Hajizadeh, N. R., Franklin, J. M., Jeffries, C. M. & Svergun, D. I. (2017). *J. Appl. Cryst.* **50**, 1212–1225.
Fournier, A. E., GrandPré, T. & Strittmatter, S. M. (2001). *Nature (London)*, **409**, 341–346.
Glaser, F., Pupko, T., Paz, I., Bell, R. E., Bechor-Shental, D., Martz, E. & Ben-Tal, N. (2003). *Bioinformatics*, **19**, 163–164.
Halff, E. F., Versteeg, M., Brondijk, T. H. C. & Huizinga, E. G. (2014). *Protein Expr. Purif.* **99**, 27–34.
He, X. L., Bazan, J. F., McDermott, G., Park, J. B., Wang, K., Tessier-Lavigne, M., He, Z. & Garcia, K. C. (2003). *Neuron*, **38**, 177–185.
Himanen, J.-P., Rajashankar, K. R., Lackmann, M., Cowan, C. A., Henkemeyer, M. & Nikolov, D. B. (2001). *Nature (London)*, **414**, 933–938.
Kabsch, W. (2010). *Acta Cryst.* D**66**, 125–132.
Kolodkin, A. L. & Tessier-Lavigne, M. (2011). *Cold Spring Harb. Perspect. Biol.* **3**, a001727.
Konarev, P. V., Volkov, V. V., Sokolova, A. V., Koch, M. H. J. & Svergun, D. I. (2003). *J. Appl. Cryst.* **36**, 1277–1282.
Kong, Y., Janssen, B. J. C., Malinauskas, T., Vangoor, V. R., Coles, C. H., Kaufmann, R., Ni, T., Gilbert, R. J. C., Padilla-Parra, S., Pasterkamp, R. J. & Jones, E. Y. (2016). *Neuron*, **91**, 548–560.
Krissinel, E. & Henrick, K. (2007). *J. Mol. Biol.* **372**, 774–797.
Laurén, J., Hu, F., Chin, J., Liao, J., Airaksinen, M. S. & Strittmatter, S. M. (2007). *J. Biol. Chem.* **282**, 5715–5725.
Lee, H., Raiker, S. J., Venkatesh, K., Geary, R., Robak, L. A., Zhang, Y., Yeh, H. H., Shrager, P. & Giger, R. J. (2008). *J. Neurosci.* **28**, 2753–2765.
Liu, B. P., Fournier, A., GrandPré, T. & Strittmatter, S. M. (2002). *Science*, **297**, 1190–1193.
Markley, J. L. (1975). *Acc. Chem. Res.* **8**, 70–80.
McCoy, A. J., Grosse-Kunstleve, R. W., Adams, P. D., Winn, M. D., Storoni, L. C. & Read, R. J. (2007). *J. Appl. Cryst.* **40**, 658–674.
McGee, A. W. & Strittmatter, S. M. (2003). *Trends Neurosci.* **26**, 193–198.
McGee, A. W., Yang, Y., Fischer, Q. S., Daw, N. W. & Strittmatter, S. M. (2005). *Science*, **309**, 2222–2226.
Meabon, J. S., De Laat, R., Ieguchi, K., Wiley, J. C., Hudson, M. P. & Bothwell, M. (2015). *J. Biol. Chem.* **290**, 9511–9520.
Mi, S., Lee, X., Shao, Z., Thill, G., Ji, B., Relton, J., Levesque, M., Allaire, N., Perrin, S., Sands, B., Crowell, T., Cate, R. L., McCoy, J. M. & Pepinsky, R. B. (2004). *Nature Neurosci.* **7**, 221–228.
Mironova, Y. A. & Giger, R. J. (2013). *Trends Neurosci.* **36**, 363–373.
Murshudov, G. N., Skubák, P., Lebedev, A. A., Pannu, N. S., Steiner, R. A., Nicholls, R. A., Winn, M. D., Long, F. & Vagin, A. A. (2011). *Acta Cryst.* D**67**, 355–367.
Pasterkamp, R. J., Anderson, P. N. & Verhaagen, J. (2001). *Eur. J. Neurosci.* **13**, 457–471.
Raiker, S. J., Lee, H., Baldwin, K. T., Duan, Y., Shrager, P. & Giger, R. J. (2010). *J. Neurosci.* **30**, 12432–12445.
Robak, L. A., Venkatesh, K., Lee, H., Raiker, S. J., Duan, Y., Lee-Osbourne, J., Hofer, T., Mage, R. G., Rader, C. & Giger, R. J. (2009). *J. Neurosci.* **29**, 5768–5783.
Saha, N., Kolev, M. V., Semavina, M., Himanen, J. & Nikolov, D. B. (2011). *Biochem. Biophys. Res. Commun.* **413**, 92–97.
Schuck, P. (2000). *Biophys. J.* **78**, 1606–1619.
Semavina, M., Saha, N., Kolev, M. V., Goldgur, Y., Giger, R. J., Himanen, J. P. & Nikolov, D. B. (2011). *Protein Sci.* **20**, 684–689.
Shao, Z., Browning, J. L., Lee, X., Scott, M. L., Shulga-Morskaya, S., Allaire, N., Thill, G., Levesque, M., Sah, D., McCoy, J. M., Murray, B., Jung, V., Pepinsky, R. B. & Mi, S. (2005). *Neuron*, **45**, 353–359.
Stephany, C.-É., Ikrar, T., Nguyen, C., Xu, X. & McGee, A. W. (2016). *J. Neurosci.* **36**, 11006–11012.
Svergun, D. I. (1992). *J. Appl. Cryst.* **25**, 495–503.
Tang, S., Woodhall, R. W., Shen, Y. J., deBellard, M. E., Saffell, J. L., Doherty, P., Walsh, F. S. & Filbin, M. T. (1997). *Mol. Cell. Neurosci.* **9**, 333–346.
Vangone, A. & Bonvin, A. M. J. J. (2015). *Elife*, **4**, e07454.
Venkatesh, K., Chivatakarn, O., Lee, H., Joshi, P. S., Kantor, D. B., Newman, B. A., Mage, R., Rader, C. & Giger, R. J. (2005). *J. Neurosci.* **25**, 808–822.
Vilar, M., Charalampopoulos, I., Kenchappa, R. S., Reversi, A., Klos-Applequist, J. M., Karaca, E., Simi, A., Spuch, C., Choi, S., Friedman, W. J., Ericson, J., Schiavo, G., Carter, B. D. & Ibáñez, C. F. (2009). *J. Cell Sci.* **122**, 3351–3357.
Vilar, M., Charalampopoulos, I., Kenchappa, R. S., Simi, A., Karaca, E., Reversi, A., Choi, S., Bothwell, M., Mingarro, I., Friedman, W. J., Schiavo, G., Bastiaens, P. I. H., Verveer, P. J., Carter, B. D. & Ibáñez, C. F. (2009). *Neuron*, **62**, 72–83.

Vilar, M., Sung, T.-C., Chen, Z., García-Carpio, I., Fernandez, E. M., Xu, J., Riek, R. & Lee, K.-F. (2014). *PLoS Biol.* **12**, e1001918.
Wang, K. C., Kim, J. A., Sivasankaran, R., Segal, R. & He, Z. (2002). *Nature (London)*, **420**, 74–78.
Wang, K. C., Koprivica, V., Kim, J. A., Sivasankaran, R., Guo, Y., Neve, R. L. & He, Z. (2002). *Nature (London)*, **417**, 941–944.
Weinreb, P. H. *et al.* (2010). *Biotechnol. Appl. Biochem.* **57**, 31–45.
Wen, D., Wildes, C. P., Silvian, L., Walus, L., Mi, S., Lee, D. H. S., Meier, W. & Pepinsky, R. B. (2005). *Biochemistry*, **44**, 16491–16501.
Wong, S. T., Henley, J. R., Kanning, K. C., Huang, K.-H., Bothwell, M. & Poo, M.-M. (2002). *Nature Neurosci.* **5**, 1302–1308.
Yun, R. H., Anderson, A. & Hermans, J. (1991). *Proteins*, **10**, 219–228.